

1. Baseline Predictions for Electrons From Heavy Flavor Decays and Drell-Yan Production at RHIC II

Ramona Vogt, LBNL and UC Davis

The theoretical prediction of the electron spectrum at Fixed-Order Next-to-Leading Logarithm, FONLL, is described in Ref. [1]. The calculation includes three main components: the p_T and rapidity distributions of the heavy quark Q in pp collisions at $\sqrt{S} = 200$ GeV, calculated in perturbative QCD; fragmentation of the heavy quarks into heavy hadrons, H_Q , described by phenomenological input extracted from e^+e^- data; and the decay of H_Q into electrons according to spectra available from other measurements. This cross section is schematically written as

$$\frac{E d^3\sigma(e)}{dp^3} = \frac{E_Q d^3\sigma(Q)}{dp_Q^3} \otimes D(Q \rightarrow H_Q) \otimes f(H_Q \rightarrow e),$$

where the symbol \otimes denotes a generic convolution. The electron decay spectrum term $f(H_Q \rightarrow e)$ also implicitly accounts for the proper branching ratio.

The decay of the D and B mesons into electrons is controlled by the experimentally measured decay spectra and branching ratios (BR). The spectrum for primary $B \rightarrow e$ decays has been measured recently by BaBar and CLEO. We fit these data and assume the same fit to apply to all bottom hadrons. Preliminary CLEO data on the inclusive electron spectrum in semi-leptonic D decays have also been fitted and assume it to be identical for all charm hadrons. Finally, the contribution of electrons from the secondary B decays $B \rightarrow D \rightarrow e$ has also been accounted for. The relevant electron spectrum is a convolution of the $D \rightarrow e$ spectra with a parton-model prediction for the $b \rightarrow c$ decay. The resulting electron spectrum is very soft, suggesting that its contribution to the total is most likely negligible.

To normalize the decay spectra, we use the branching ratios for bottom and charm hadron mixtures appropriate to this high energy regime: $\text{BR}(B \rightarrow e) = 10.86 \pm 0.35\%$, $\text{BR}(D \rightarrow e) = 10.3 \pm 1.2\%$, and $\text{BR}(B \rightarrow D \rightarrow e) = 9.6 \pm 0.6\%$. Although the results are shown here for electrons, the same decay spectra and branching ratios are assumed to be valid for decays to muons as well.

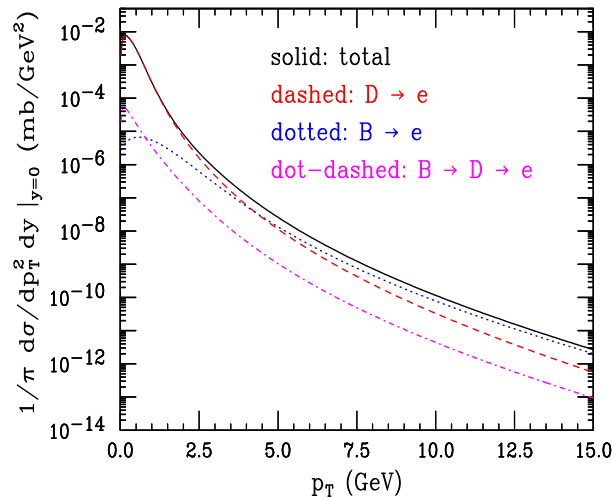


Fig. 1: The components of the electron transverse momentum spectrum calculated with the central mass and scale values: $m_c = 1.5$ GeV, $m_b = 4.75$ GeV and $\mu_{R,F}/m_T = 1$.

Figure 1 shows the contributions from $D \rightarrow e$, $B \rightarrow e$ and $B \rightarrow D \rightarrow e$ decays as well as the total at $\sqrt{S} = 200$ GeV for the central values of $m_c = 1.5$ GeV, $m_b = 4.75$ GeV and $\mu_F = \mu_R = m_T \equiv \sqrt{p_T^2 + m_Q^2}$. The results are calculated in the midrapidity range $|y| \leq 0.75$. As anticipated, the

$B \rightarrow D \rightarrow e$ secondary electron spectrum is extremely soft, only exceeding the primary $B \rightarrow e$ decays at $p_T < 1$ GeV, and always negligible with respect to the total yield.

The electron contribution from B decays becomes larger than that of electrons from D decays at $p_T \simeq 4$ GeV for the central values. This cross over is rather sensitive to the mass and scale values chosen, as shown in Fig. 2, for $\sqrt{s} = 200$ and 500 GeV. The theoretical uncertainty bands shown in Ref. [1] for charm and bottom quarks as well as D and B mesons are replicated in Fig. 2 for the decays to leptons. Depending on the quark mass and scale, the cross over can begin at electron p_T values as low

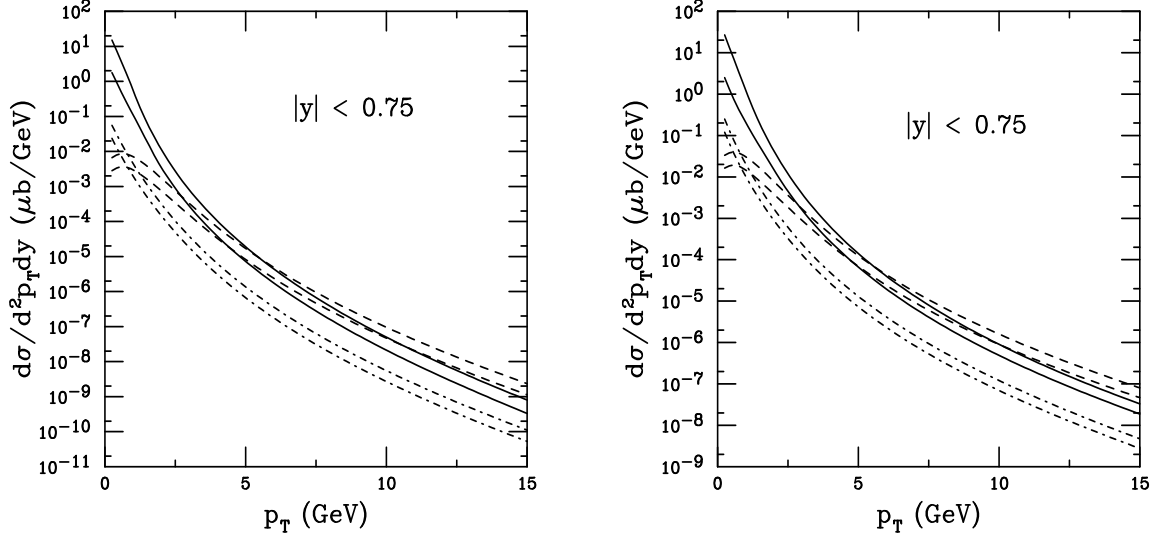


Fig. 2: The theoretical FONLL bands for $D \rightarrow eX$ (solid), $B \rightarrow eX$ (dashed) and $B \rightarrow DX \rightarrow eX'$ (dot-dashed) as a function of p_T in $\sqrt{s} = 200$ GeV (left-hand side) and 500 GeV (right-hand side) pp collisions for $|y| < 0.75$.

as 2.5 GeV up to values as high as 12 GeV. The cross over point is not strongly dependent on the energy. The low p_T value at which the theoretical uncertainty bands begin to cross is similar. However, since the bottom cross section is increasing faster with energy than the charm cross section, the upper value of p_T at which the cross over occurs is decreased to $p_T \sim 10$ GeV. Therefore to separate charm decay leptons from bottom decay leptons in the region $2.5 < p_T < 10 - 12$ GeV, it is imperative to measure the charm and bottom cross sections by an alternative method such as direct reconstruction of hadronic decay channels.

Figure 3 shows the theoretical uncertainty band for electrons coming from charm and bottom hadron decays at $\sqrt{s} = 200$ GeV at RHIC. The sum of the three components shown in Fig. 1 corresponds to the central value of the band in Fig. 3. The upper and lower limit of the band are obtained by summing the upper and lower limit for each component.

We only show the midrapidity results for the electrons from heavy flavor decays in the FONLL approach. The decay electrons in the region $|y| \leq 0.75$ come from charm and bottom hadrons with $|y| \leq 2$. We cannot calculate the decay leptons in the forward and backward regions in this approach since the matching of the resummed and fixed order calculations does not work well at forward rapidities and, for $y > 2.5$ the FONLL result begins to break down. As shown in the talk on heavy flavor production, the NLO and FONLL results are rather similar except at $p_T > 10 - 12$ GeV when the large logs of p_T/m_Q artificially increase the NLO cross section. Thus it might be feasible to estimate the lepton decay spectra at forward rapidities at NLO rather than FONLL.

In this talk, we also discussed Drell-Yan production in pp and d+Au collisions, calculated to next-to-leading order (NLO). The lepton pair continuum calculation includes virtual photon exchange, virtual Z^0 exchange and γ^*-Z^0 interference, see Ref. [2] for details of the calculation. The virtual

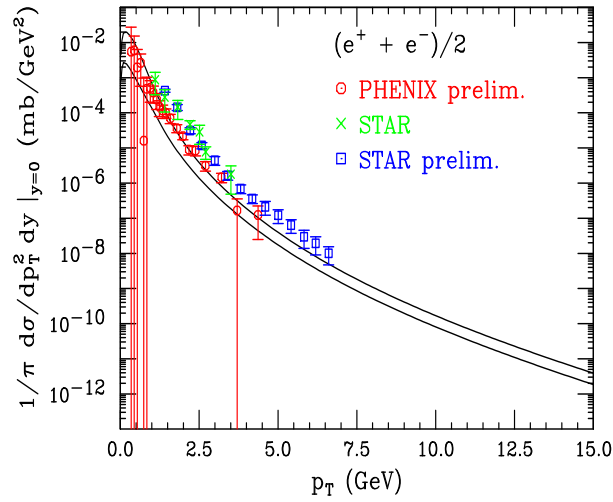


Fig. 3: Prediction for the theoretical uncertainty band of the electron spectrum from charm and bottom in pp collisions compared to data from PHENIX (preliminary) and STAR (final and preliminary).

photon exchange is dominant at masses accessible at RHIC energies. We calculated the mass distribution in the range $2 < M < 20$ GeV, where M is the mass of the lepton pair, for several rapidity bins: $-2.2 < y < -1.2$, $|y| \leq 1$ and $1.2 < y < 2.2$. The bins forward and backward of midrapidity correspond to the coverage of the PHENIX muon arms. We also calculated the rapidity distribution for $|y| \leq 2.5$ in several mass bins: $2 < M < 3$ GeV, $4 < M < 9$ GeV and $11 < M < 20$ GeV. The lowest mass bin is below the J/ψ peak, the intermediate bin is between the J/ψ and Υ mass regions and the highest mass bin is above the Υ region. We calculated the results in pp collisions at $\sqrt{S} = 200$ and 500 GeV and d+Au collisions at 200 GeV.

The d+Au calculations also include the EKS98 and FGS parameterizations of nuclear shadowing. The FGS parameterization includes an upper and lower bound on the amount of gluon shadowing but uses the same parameterization for the sea quarks. The FGS parameterization of sea quark shadowing is weaker than that of EKS98 for momentum fractions, x , in the range $2 \times 10^{-4} < x < 0.2$, becoming unity for $x \geq 0.2$. At lower values of x the FGS parameterization has stronger shadowing than EKS98. On the other hand, the EKS98 sea quark parameterization is shadowed over the whole x range. The FGS and EKS98 valence quark parameterizations are identical, showing shadowing for $x < 0.02$ and antishadowing for $0.02 < x < 0.4$ with an EMC shadowing region for higher x .

A comparison of the pp and d+Au mass and rapidity distributions shows that the shapes are different due to isospin effects, even before shadowing is taken into account. In the low mass and mid-to-forward rapidity regions, shadowing dominates over isospin. However, for masses greater than 10 GeV, isospin effects tend to dominate.

In the x region accessible at RHIC, effects of gluon shadowing on Drell-Yan production are negligible. This can be understood by studying the K factors, the ratios of the NLO to leading order cross sections, as a function of pair mass and rapidity. The K factors, indicative of the size of the NLO corrections, are on the order of 1.4 at the lowest masses and increase slowly with rapidity. At higher masses, the increase of the K factor at 200 GeV is an indication of the approach of the edge of phase space where the corrections become larger. (This increase is significantly less for 500 GeV collisions.) The contribution of initial-state gluons from the $qg \rightarrow \gamma^*q$ process is only a fraction of the total NLO correction, $\sigma[\mathcal{O}(\alpha_s)] \approx (K - 1)\sigma[\mathcal{O}(\alpha^2)]$, which also includes the virtual corrections to the LO cross section and the real correction, $q\bar{q} \rightarrow \gamma^*g$. Since Drell-Yan production is thus dominated by $q\bar{q}$ initial states, it is not surprising that the shadowing results for the p_T -integrated mass and rapidity distributions reflect only quark shadowing.

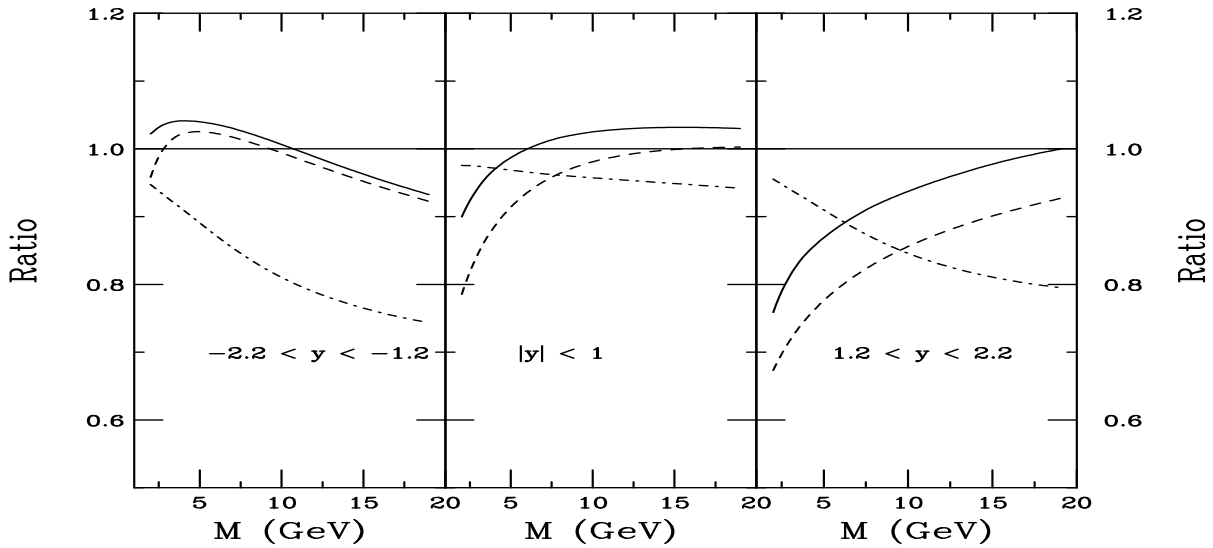


Fig. 4: The dilepton shadowing and isospin ratios at 200 GeV in the rapidity windows: $-2.2 < y < -1.2$ (left); $|y| < 1$ (center); and $1.2 < y < 2.2$ (right). The shadowing results, the ratios with to without shadowing are given by the solid (FGS) and dashed (EKS98) curves while the dot-dashed curve is the d+Au/pp ratio without shadowing.

Figure 4 shows the ratios of d+Au with shadowing included to those without shadowing in the solid (FGS) and dashed (EKS98) curves. The results as a function of mass are shown in the 3 rapidity bins: backward (left), midrapidity (center) and forward (right). The two parameterizations give the most similar results in the backward region where x_2 is largest since this region has a large valence quark contribution and valence quark shadowing is identical for the two cases. There is an antishadowing bump at the lowest masses, leading to an EMC region for $M > 10$ GeV. (For $M = 4$ GeV, $-2.2 < y < -1.2$ corresponds to $0.18 > x_2 > 0.066$ while for $M = 10$ GeV, $0.45 > x_2 > 0.17$ at leading order where $x_2 = (M/\sqrt{S}) \exp(-y)$.) At midrapidity, some low x shadowing is exhibited for $M < 5$ GeV for FGS and for $M < 12$ GeV for EKS98. In the most forward rapidity bin, both parameterizations show low x shadowing over the full mass range. (Here for $M = 4$ GeV, $1.2 < y < 2.2$ corresponds to $0.006 > x_2 > 0.0022$ while $M = 10$ GeV corresponds to $0.015 > x_2 > 0.0055$.) Note that in the x regime relevant here, the EKS98 sea quark shadowing is always stronger than the FGS parameterizations.

Also shown in Fig. 4 in the dot-dashed curves are the d+Au/pp ratios without shadowing. This isospin ratio needs to be folded into a measurement to properly extract the shadowing contribution. Since x increases with M , the isospin effect grows with M . It is asymmetric around $y = 0$, as evident from the stronger effect in the backwards rapidity bin at large masses. The difference arises because the charge-to-mass ratio, Z/A , is not the same for deuterons and gold. The effect is smallest at midrapidity because both $x_1 = (M/\sqrt{S}) \exp(y)$ and x_2 are similar whereas in the forward and backward regions, x grows large for one of the colliding nuclei. In the forward region, x_1 is large for the deuteron while, in the backward region, x_2 is large for the gold nucleus.

The calculated ratios are shown as a function of rapidity in the three mass bins in Fig. 5. In the smallest mass bin, the shadowing effects are largest, increasing from a slight antishadowing effect at large negative rapidity to a small x shadowing effect at large positive rapidity. By the largest mass bin, there is evidence of an EMC region at large negative rapidity and only a small shadowing effect at positive rapidity. Again the isospin effect is seen to increase with mass. It is not symmetric around $y = 0$, as seen also in Fig. 4 but is largest for large $|y|$ and small at $y \sim 0$.

While studies of Drell-Yan production in pp and d+Au collisions could help understand quark shadowing in more detail and at higher scales than previously available, experimental extraction of the Drell-Yan contribution will not be easy. In addition, the nuclear isospin needs to be accounted for prop-

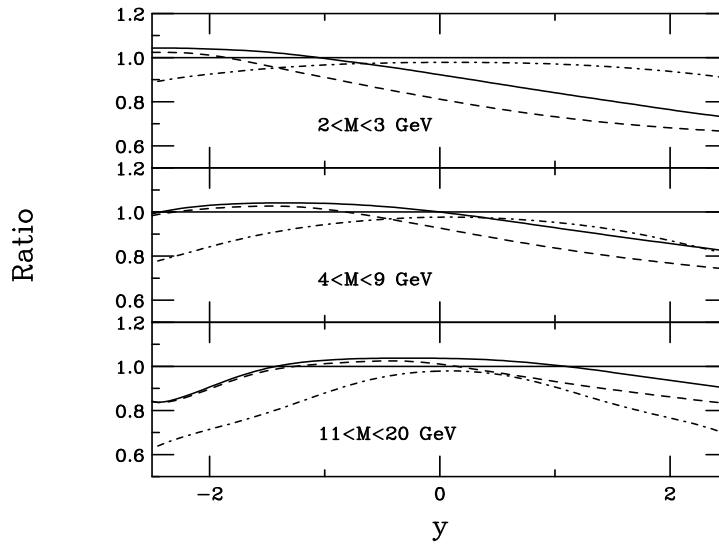


Fig. 5: The dilepton shadowing and isospin ratios at 200 GeV in the mass windows: $2 < M < 3$ GeV (top); $4 < M < 9$ GeV (center); and $11 < M < 20$ GeV (bottom). The shadowing results, the ratios with to without shadowing are given by the solid (FGSh) and dashed (EKS98) curves while the dot-dashed curve is the d+Au/pp ratio without shadowing.

erly to extract the shadowing effects.

References

- [1] M. Cacciari, P. Nason and R. Vogt, hep-ph/0502203.
- [2] A. Accardi *et al.*, hep-ph/0308248.